SUPPLEMENTAL MATERIAL

Left-Right Symmetry Breaking in Tissue Morphogenesis via Cytoskeletal Mechanics

Ting-Hsuan Chen, Jeffrey J. Hsu, Xin Zhao, Chunyan Guo, Margaret Wong, Yi Huang, Zongwei Li, Alan Garfinkel, Chih-Ming Ho, Yin Tintut, Linda L. Demer

From the Mechanical and Aerospace Engineering Department (T.-H.C., Y.H., C.-M.H.), Department of Medicine (J.J.H., A.G., Y.T., L.L.D.), Department of Bioengineering (M.W., C.-M.H., L.L.D.), and Department of Integrative Biology and Physiology (A.G., L.L.D.), University of California Los Angeles, Los Angeles, California, USA; Institute of Robotics & Automatic Information System (X.Z., C.G., Z.L.), Nankai University, Tianjin, China.

Short Title:
Left-right asymmetry in vascular cells

Correspondence to:
Linda L. Demer
Department of Medicine, University of California Los Angeles
10833 LeConte Avenue
Los Angeles, CA 90095-1679
Phone: (310) 206-2677 (office)
FAX: (310) 825-4963
Email: Ldemer@mednet.ucla.edu

Detailed Methods

Micropatterning. A glass substrate (Precise Glass and Optics, CA) was cleaned and coated with HMDS, followed by spin-coating with photoresist (AZ4620). The photoresist was exposed by ultraviolet, developed (AZ-400K), and treated with oxygen plasma (500 mTorr, 200 W) for 2 min. The remaining photoresist was rinsed with acetone, IPA, and deionized water. For PEG coating, the HMDS/glass substrates were immersed in 3 mM of $C_3H_9O_3Si(C_2H_4O)_{6\text{-}9}CH_3$ (Gelest, Inc., PA) dissolved in anhydrous toluene with 1% triethylamine (v/v) (Sigma-Aldrich, St. Louis, MO) for 4 hours, followed by ultrasonication in anhydrous toluene, ethanol and deionized water for 5 min, respectively.[1] After drying, the HMDS/PEG substrates were diced into 2 cm × 2 cm chips and stored in desiccators. Prior to plating cells, the HMDS/PEG substrates were first incubated with FN solution (50 µg/ml, Sigma-Aldrich, St. Louis, MO) in calcium-/magnesium-free phosphate-buffered saline (Mediatech, Inc., VA) at 4°C for 15 min. The same protocol was used for other ECM proteins including collagen types I and IV (Santa Cruz Biotechnology, Inc., CA) and laminin-1 (Sigma-Aldrich, St. Louis, MO). The protein-coated chip was plated with VMCs (200,000 cells per chip), BVECs (400,000 cells per chip), 3T3 cells (300,000 cells per chip), or ST2 cells (200,000 cells per chip) for 30 min in 500 µl media. After brief washings, only cells adhering to the ECM regions remained. The FN/PEG interface was identified by either titanium lines (for multicellular pattern formation, orientation analysis, and time-lapse videomicroscopy) or etched microgrooves (for assays of polarity and stress fiber) on the reverse side of the chip fabricated before the preparation of ECM/PEG substrates.

Shadow-mask plating. The mask was made of stainless steel (2 cm × 2 cm × 100 µm, NW Etch, WA) containing 25 parallel windows (300 µm × 1.5 cm) spaced 300 µm apart. Prior to plating, the tissue culture dish was first uniformly coated with FN solution (50 µg/ml) at 4°C for 15 min. After brief washings, a permanent magnet was attached underneath the culture dish to immobilize the mask. Thereafter, cells were plated through the mask for 30 min (200,000 cells in 500 µl) followed by removal of the shadow-mask. Schematic diagram for detailed procedure and results are provided in Online Figure VIII.

Cell culture. VMCs, BVECs, and 3T3 cells were isolated and cultured as described[2-4] and ST2 cells were commercially purchased (Cell Bank, Riken Bioresource Center, Japan). All cells were grown in Dulbecco's Modified Eagle's Medium supplemented with 15% heat inactivated fetal bovine serum and 1% penicillin/streptomycin (10,000 I.U./10,000 µg/ml; all from Mediatech, Inc., VA). Cells were incubated at 37° C in a humidified incubator (5% CO_2 and 95% air) and passaged every three days.

Multicellular pattern formation. Each culture was prepared on one of four substrates: 1) 35-mm plastic dishes, 2) binary substrates consisting of PEG alternating with purified ECM protein (FN, collagen

I, collagen IV, or laminin-1), 3) uniformly coated FN substrate on chips with titanium on the reverse side of chip, or 4) shadow-mask plating as described elsewhere in methods, with media changes every three days. For inhibition of stress fiber or intervention of morphogen activities, Y27632 (10 µM, Ascent Scientific, NJ), blebbistatin (10 µM, Sigma-Aldrich, St. Louis, MO), BMP-2 (200 ng/ml, R&D systems, MN), noggin (100 ng/ml, R&D systems, MN), and warfarin (50 µM, Sigma-Aldrich, St. Louis, MO) were added at day zero and replenished with each media change. After 10-14 days, cultures were stained with hematoxylin (Sigma-Aldrich, St. Louis, MO) for 15 min to reveal multicellular aggregates. The panorama images (1.5 cm × 1.5 cm in visual field) were taken using a series of images (4.4 mm × 3.3 mm in visual field) with 1-2 mm offset, and recombined by panoramic stitching software (PTGui, New House Internet Services BV, Rotterdam, Netherlands). Images were acquired using an inverted microscope (Olympus IX71) with a color digital bio-imaging camera (Exi Aqua) in bright field.

Green fluorescent protein transfection. VMCs were transfected with a plasmid encoding GFP (pmaxGFP; Amaxa Biosystems, Germany) using the Effectene Transfection Reagent (Qiagen, CA). One day prior to transfection, 500,000 cells were plated on a 60-mm plastic culture dish. For transfection, the GFP plasmid was mixed with the transfection reagent following the manufacturer's instructions and applied to the cells for 3 days. Each image was captured using the CCD (Coolsnap ES, Photometrics, AZ) equipped with an inverted microscope (Eclipse TE 2000, Nikon Instruments Inc., CA) with an excitation wavelength of 420-495 nm.

Time-lapse videomicroscopy. Cultures were incubated in a microscopic thermal stage (HCS60, Instec, Inc., CO) at 37° C and continuously supplied with premixed 5% CO_2. Images were acquired at 5 min intervals for a total of 22.5 hours using the CCD and inverted microscope (as above) in bright field. To verify adequacy of the on-stage incubator, proliferation of 3T3 cells in the thermal stage was compared with that in a conventional incubator by hemocytometry. Over 100 hours of culture, proliferation in the thermal stage remained comparable to that in the conventional incubator (Online Figure X).

Immunofluorescent staining. Cells were cultured on FN/PEG substrates or shadow-mask plated in normal growth medium, or on FN/PEG substrates in growth medium supplemented with Y27632 (10 µM) or blebbistatin (10 µM). FN/PEG stripes were 600 µm wide for the polarity assay and 300 µm for stress fiber distribution. Cells were fixed in cold methanol (-20° C) for 10 min, blocked with Image-iT™ FX signal enhancer (Invitrogen, CA) at room temperature for 30 min, then labeled with monoclonal anti-α-tubulin-FITC antibody (Sigma-Aldrich, St. Louis, MO; 1:50; for polarity assay on VMCs and BVECs), pericentrin polyclonal antibody (Covance, CA; 1:500; for polarity assay on 3T3 cells and ST2 cells), or NMM-IIa antibody (Covance, CA; 1:1000; for stress fiber distribution on all cells) at room temperature for 1 hour. The pericentrin and NMM-IIa antibodies were subsequently labeled with secondary antibodies for 30 min (Alexa Fluor 555 anti-rabbit IgG antibodies, Invitrogen, CA; 1:500). Samples were mounted by ProLong GOLD antifade with DAPI (Invitrogen, CA). Images were acquired using the CCD and inverted microscope (as above) with appropriate excitation wavelengths (420-495 nm for anti-α-tubulin-FITC; 510-560 nm for NMM-IIa and pericentrin; and 330-380 nm for DAPI). For stress fiber distribution of NMM-IIa, images were stacked using etched microgrooves on the reverse surface for registration. For shadow-mask plating experiments, images were stacked using automated edge detection for registration (described below). After stacking images, NMM-IIa distributions were represented as the intensity value normalized by the number of images, and the scale bar in different conditions was scaled to the same maximum/minimum value in the control.

Orientation analysis. Images were processed using image segmentation, boundary tracing, and orientation calculation. Specifically, given the intensity histogram from a gray scale image of a GFP-transfected cell (Online Figure XI A), we identified the peak frequency (gray level 75 in Online Figure XI B) as the representative value for background, and the second peak (gray level 255 in Online Figure XI B) as the representative value for cells. To segment the image into binary images, the threshold for image segmentation was set at the midpoint between these two peaks (Online Figure XI C). Next, a boundary tracing algorithm, using an 8-connected neighborhood, was applied to locate the contours of bright regions, allowing identification of cells based on the size of the closed-loop regions. The orientation angle was calculated by the method of "minimum circumscribed rectangle" in which the shape of a given cell (blue region in Online Figure XI D) can be approximated by circumscribing rectangles of different sizes (position 1, 2, or 3 in Online Figure XI D). Thus, the orientation angle, θ, was defined as the longitudinal axis of the rectangle of minimal area relative to the horizontal axis of the image (i.e. the axis of the interface demarcated by the black titanium line; position 3 in Online Figure XI D). Finally, the histogram of θ distribution was determined over all GFP-transfected cells (Online Figure XI E).

Stacking images of immunofluorescence NMM-IIa after shadow-mask plating. Due to the absence of a conventional registration marker, immunofluorescence images for NMM-IIa after shadow-plating were aligned to achieve registration using automated edge detection (Online Figure XII A). Specifically, as for orientation analysis above, a segmentation threshold was defined by the midpoint between the frequency peaks for cells and background (Online Figure XII B). Automated boundary tracing was then applied to locate the contours of bright regions, and the sheet of cells was identified by excluding small closed-loop regions. Subsequently, the edges of each cell sheet were identified by plotting the number of bright pixels as a function of row index of the image (blue curve in Online Figure XII C). We selected a level of 300 bright pixels as the threshold to identify the edge of the cell sheet (red dotted line in Online Figure XII C). In each image, the upper and lower edges of the cell sheet were defined by the two intersections of the red dashed line with the blue curve (Online Figure XII C). The midline of the cell sheet, defined as equidistant between two edges, was used to register and stack the images (Online Figure XII D).

Mathematical model. The reaction-diffusion phenomenon was qualitatively modeled by a system of partial differential equations. VMCs secrete two morphogens, the slowly-diffusing activator, BMP-2, and its rapidly-diffusing inhibitor, MGP. Over this 2-dimensional domain, the reaction and diffusion of these morphogens create a spatiotemporal pattern of morphogenetic activities that mediate pattern formation. Specifically, the production of BMP-2 obeys an autocatalytic reaction and saturates at a high level of BMP-2. BMP-2 induces expression of MGP and is inhibited by MGP. The morphogen activities are proportional to cell density and also subject to degradation.[5] Under the influence of these chemical activities, cells proliferate, diffuse in proportion to local cell density, and chemotactically migrate along a gradient of BMP-2 activity.[6, 7]

Based on the above, cell density and activities of the activator and inhibitor were formulated as functions of space, $N(x, y)$, $a(x, y)$, and $h(x, y)$, respectively:

$$\frac{\partial a}{\partial t} = D_a \nabla^2 a + \frac{N\rho_a a^2}{h(1+q^2a^2)} - \mu_a a \tag{1}$$

$$\frac{\partial h}{\partial t} = D_h \nabla^2 h + N\rho_h a^2 - \mu_h h \tag{2}$$

$$\frac{\partial N}{\partial t} = D_N \nabla^2 N - \nabla \cdot \left(\frac{\chi N}{(k_N + a)^2} \nabla a \right) + r_N N\left(1 - \frac{N}{N_c}\right) \tag{3}$$

D_a and D_h are the diffusion coefficients of activator and inhibitor, and D_N is the coefficient of cytokinetic diffusion. In Equation 1, the production of activator follows an autocatalytic reaction kinetic and is also regulated by the activity of inhibitor. Therefore, we use a sigmoidal form $\rho_a a^2/(h(1+q^2a^2))$, where ρ_a is coefficient of autocatalysis and q denotes the constant for autocatalytic saturation. The inhibition of a by h is modeled by placing the h term in the denominator. In Equation 2, the production of inhibitor is formulated as a function of a^2 where ρ_h is the coefficient of this induced-reaction. In the first two equations, the production of activator and inhibitor are proportional to the cell density N and degrade in a first-order manner expressed by $\mu_a a$ and $\mu_h h$. In Equation 3, the chemotactic migration in response to the gradient of activator is regulated by the factor χ and saturates at high levels of a. k_N denotes the constant for the saturation of chemotaxis. r_N is the maximum rate of cell proliferation, and N_c is the cell density at confluence.

To derive corresponding equations that allow for migration of cells with preferred directions, the cell motility equation (Eqn. 3) may be modified by the rotation of axes **x** and **y** and weighting the migration coefficients toward one axis.[8] First, the cell motility equation may be restated as a dot product of a derivative operator and a gradient vector, which may represent the gradient of cell density or the gradient of BMP-2 in the 2-dimensional domain. Thus:

$$\begin{aligned}\frac{\partial N}{\partial t} &= \nabla \cdot [D_N \nabla N - \frac{\chi N}{(k_N + a)^2}\nabla a] + r_N N(1 - \frac{N}{N_c}) \\ &= \nabla \cdot G + r_N N(1 - \frac{N}{N_c})\end{aligned} \qquad 4$$

where ***G*** represents the combinatory gradient vector consisting of the gradient of cell density and BMP-2. While the axes **x** and **y** are rotated to (cosθ, sinθ) and (-sinθ, cosθ) (red axes in Figure 4A), ***G*** is decomposed with respect to these rotated axes to allow scaling of directional coefficients. To scale anisotropic migration in the rotated axes, the directional coefficients, b_1 and b_2, were introduced for the decomposed vectors in rotated axes (cosθ, sinθ) and (-sinθ, cosθ), respectively. The scaled gradient vector, ***G***, is then rearranged with respect to the original axes **x** and **y**. The above may be summarized as follows:

$$\begin{aligned}G_m{}^T &= RFR^T G^T \\ F &= \begin{bmatrix} b_1 & 0 \\ 0 & b_2 \end{bmatrix}\end{aligned} \qquad 5$$

where ***G_m*** means the modified gradient vector ***G***, ***F*** is the matrix of directional coefficients , and ***R*** is the rotational matrix. With this modified gradient vector, the temporal variation of *N* is recalculated by the dot product of derivative operator and the modified gradient vector:

$$\begin{aligned}\frac{\partial N}{\partial t}&=\nabla\cdot G_m++r_N N(1-\frac{N}{N_c})\\&=\sum\nolimits_{ij}A_{ij}[\nabla^T\otimes(D_N\nabla N-\frac{\chi N}{(k_N+a)^2}\nabla a)]_{ij}+r_N N(1-\frac{N}{N_c})\\A&=\begin{bmatrix}b_1\cos^2\theta+b_2\sin^2\theta & (b_1-b_2)\cos\theta\sin\theta\\(b_1-b_2)\cos\theta\sin\theta & b_1\sin^2\theta+b_2\cos^2\theta\end{bmatrix}\end{aligned} \qquad 6$$

Of note, this modified equation is a more generalized form. The original equations of isotropic migration may be stated as a special case where $b_1 = b_2 = 1$. Together with the equations of morphogenetic dynamics, the reaction-diffusion mechanism is then described in a series of partial differential equations with anisotropic cell migration:

$$\begin{aligned}\frac{\partial a}{\partial t}&=D_a\nabla^2 a+\frac{N\rho_a a^2}{h(1+q^2a^2)}-\mu_a a\\\frac{\partial h}{\partial t}&=D_h\nabla^2 h+N\rho_h a^2-\mu_h h\\\frac{\partial N}{\partial t}&=\sum\nolimits_{ij}A_{ij}[\nabla^T\otimes(D_N\nabla N-\frac{\chi N}{(k_N+a)^2}\nabla a)]_{ij}+r_N N(1-\frac{N}{N_c})\\A&=\begin{bmatrix}b_1\cos^2\theta+b_2\sin^2\theta & (b_1-b_2)\cos\theta\sin\theta\\(b_1-b_2)\cos\theta\sin\theta & b_1\sin^2\theta+b_2\cos^2\theta\end{bmatrix}\end{aligned} \qquad 7$$

In non-dimensional form, this becomes:

$$\begin{aligned}\frac{\partial u}{\partial t^*}&=D\nabla^{*2}u+\gamma(\frac{nu^2}{v(1+ku^2)}-cu)\\\frac{\partial v}{\partial t^*}&=\nabla^{*2}v+\gamma(nu^2-ev)\\\frac{\partial n}{\partial t^*}&=\sum\nolimits_{ij}A_{ij}[\nabla^{*T}\otimes(D_n\nabla^* n-\frac{\chi_0 n}{(k_n+u)^2}\nabla^* u)]_{ij}+r_n n(1-n)\\A&=\begin{bmatrix}b_1\cos^2\theta+b_2\sin^2\theta & (b_1-b_2)\cos\theta\sin\theta\\(b_1-b_2)\cos\theta\sin\theta & b_1\sin^2\theta+b_2\cos^2\theta\end{bmatrix}\end{aligned} \qquad 8$$

where the dimensionless variables are:

$$\nabla^* = L^2\nabla\,,\ t^* = \frac{D_h}{L^2}t\,,\ u = \frac{\rho_h}{\rho_a}a\,,\ v = \frac{\rho_h}{\rho_a{}^2 N_c t_c}h\,,\ n = \frac{N}{N_c}\,,\ \gamma = \frac{L^2}{D_h t_c}\,,\ k = \frac{q^2 \rho_a{}^2}{\rho_h{}^2}\,,\ c = \mu_a t_c\,,$$

$$e = \mu_h t_c\,,\ D = \frac{D_a}{D_h}\,,\ D_n = \frac{D_N}{D_h}\,,\ \chi_0 = \frac{\rho_h}{D_h \rho_a}\chi\,,\ k_n = \frac{\rho_h}{\rho_a}k_N\,,\ r_n = \frac{L^2}{D_h}r_N\,,$$

and where L is the linear dimension of the domain, and t_c is the characteristic timescale of biosynthetic kinetics. We used this series of partial differential equations to model anisotropic cell migration as described in the text.

The partial differential equations were solved via the finite difference method. The 2-D spatial domain was discretized with a uniform mesh (200 × 200). For all simulations, non-flux boundary conditions were used, and initial values of u, v and n were uniformly distributed with a 2% random fluctuation.

Parameter values were estimated from the biological literature as described previously, with some modifications to correct for our revised culture platform and conditions.[5] The ratio of diffusivities and the degradation terms were described previously. To account for the smaller dimension of the culture plates, we reduced the domain length, L, to 1.5 cm. To allow for reduced diffusion through purified substrates, the diffusion coefficient for the inhibitory morphogen, D_h was estimated as 3×10^{-8} cm^2/sec. Using the same approximate timescale of biosynthesis (3600 seconds), the non-dimensional scaling factor, γ, becomes 20000. We estimated D_N as 2×10^{-9} cm^2/sec, as described previously.[9] Assuming cytokinetic diffusion and chemotaxis to be on the same order of magnitude, we then obtained $D_n = 0.06$ and $\chi_0 = 0.06$.[6] The chemotaxis constant, k_n, was set at 1, as suggested by the literature.[6] Using $r_N = 0.015$ hr^{-1} leads to $r_n = 322$ in dimensionless form. The total time $t^* = 1$ for each simulation.

The autocatalytic constant, k, which sets the saturating value at specific values of v, was estimated using the parametric space (Turing space) in which the pattern formation is driven by Turing instability, given that the activity of MGP in the experiments may not be measurable. The suitable range of k is calculated using the mathematic conditions that satisfy Turing space:

$$\begin{aligned} & f_u + g_v < 0 \\ & f_u g_v - f_v g_u > 0 \\ & f_u + D g_v > 0 \\ & (f_u + D g_v)^2 - 4D(f_u g_v - f_v g_u) > 0 \end{aligned} \qquad 9$$

where the subscript denotes the first-order derivative with respect to u or v. Note that the inequalities are evaluated at steady state (u_0, v_0), in which the temporal change of morphogen activities and rates of diffusion are zero. Thus, the mathematical components in the inequalities can be written as:

$$
\begin{aligned}
f_u &= \frac{2u_0}{v_0(1+ku_0{}^2)^2} - c \\
f_v &= -\frac{u_0{}^2}{v_0{}^2(1+ku_0{}^2)} \\
g_u &= 2u_0 \\
g_v &= -e.
\end{aligned}
\qquad 10
$$

The steady state values u_0 and v_0 are functions of *k*, *e* and *c*. Given $D = 0.005$, the Turing space can be plotted as function of *k* and *e*/*c* (Online Figure XIII). Based on our pre-selected values, $e/c = 2$ (red dotted line in Online Figure XIII) gives the acceptable range of *k* as $0 < k < 0.34$ (red line within the blue region in Online Figure XIII). In our simulation, we chose $k = 0.28$.

Supplemental Figures and Figure Legends

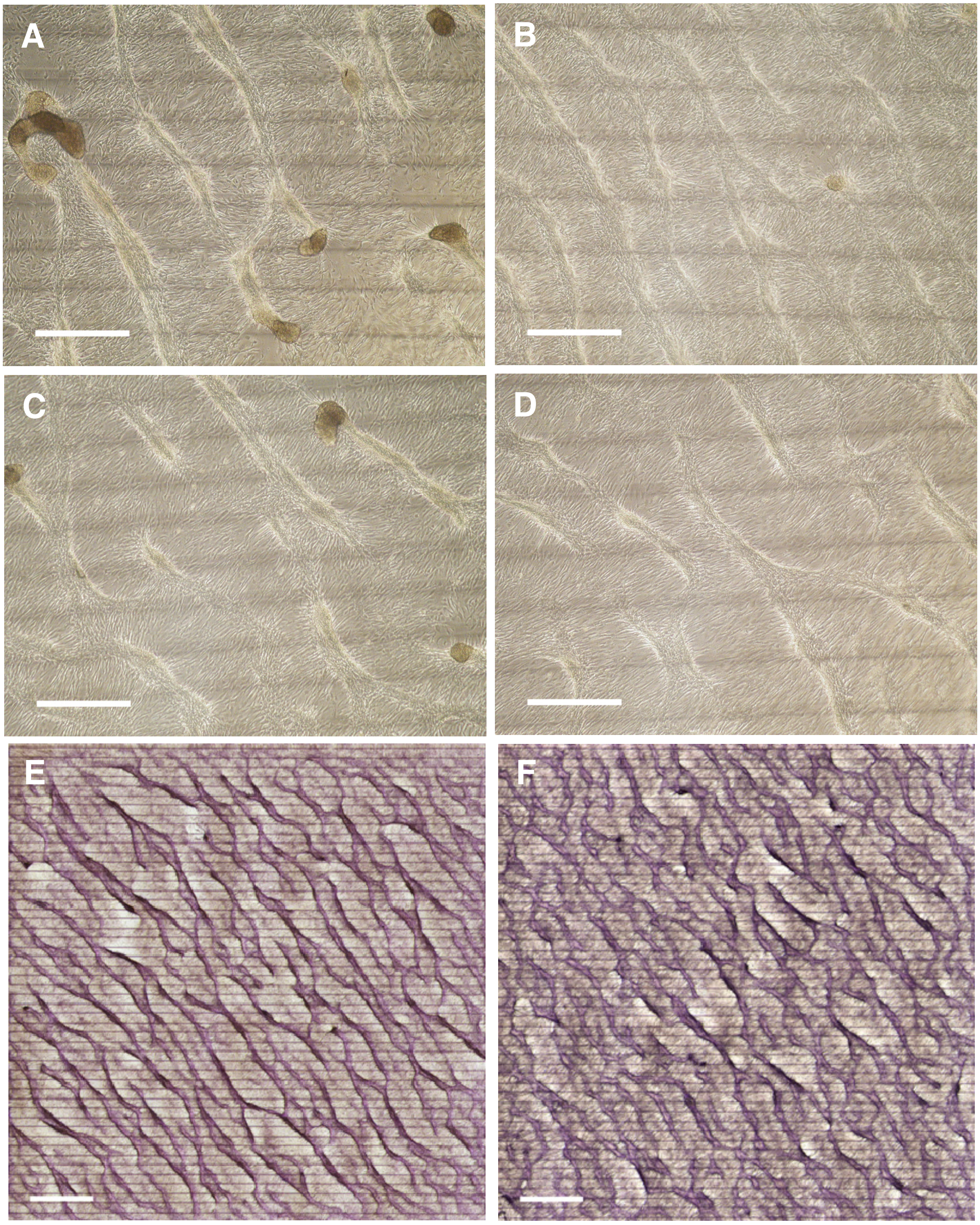

Online Figure I. The consistent LR asymmetry of ridge formation from different passages and chemical treatments. Phase contrast microscopy of multicellular ridges (**A**) in normal medium and in the presence of (**B**) exogenous BMP-2, (**C**) exogenous noggin, and (**D**) warfarin. Scale bar, 600 µm. Light microscopy of multicellular ridges stained with hematoxylin in VMCs cultured from (**E**) passage 16 and (**F**) passage 21. Scale bar, 2 mm.

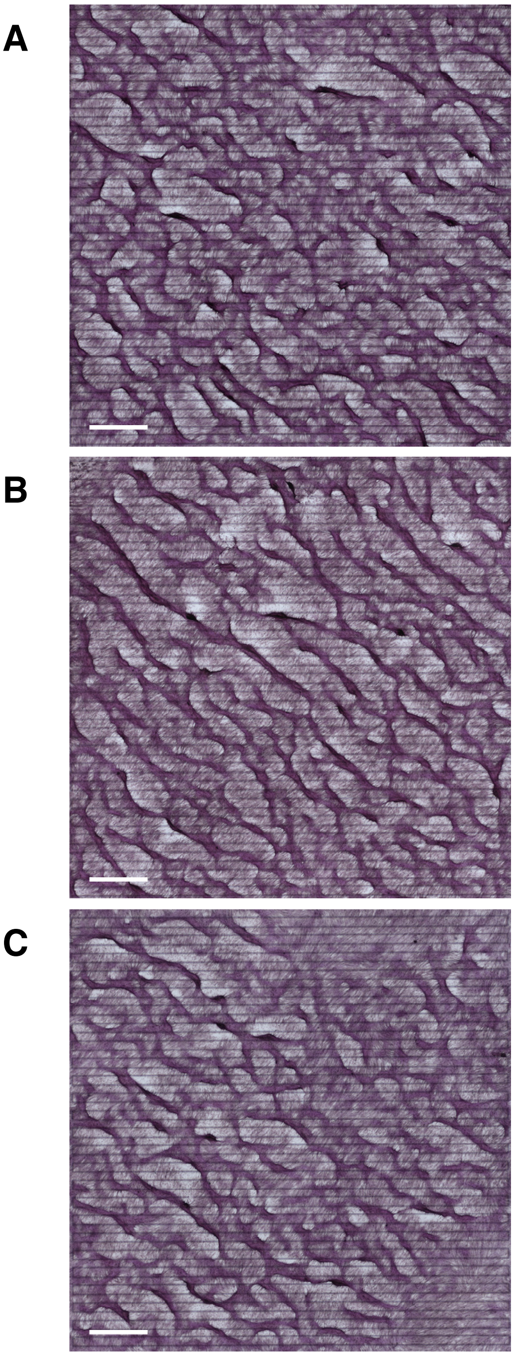

Online Figure II. Tests of matrix substrates showing persistence of LR asymmetry on extracellular matrices other than FN. Hematoxylin stain of ridges on (**A**) collagen I, (**B**) collagen IV, and (**C**) laminin-1. Scale bar, 2 mm.

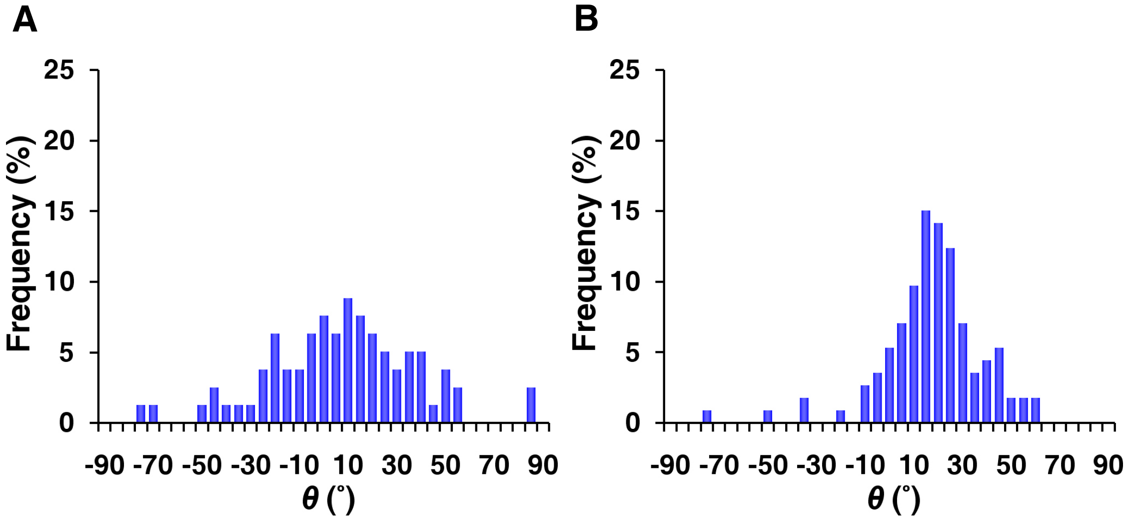

Online Figure III. Histograms of coherent orientation *θ* from day 2 and day 4. **A,** Day 2 (6 ± 30°; n = 79 cells; mean ± s.d.). **B,** Day 4 (15 ± 20°; n = 113 cells).

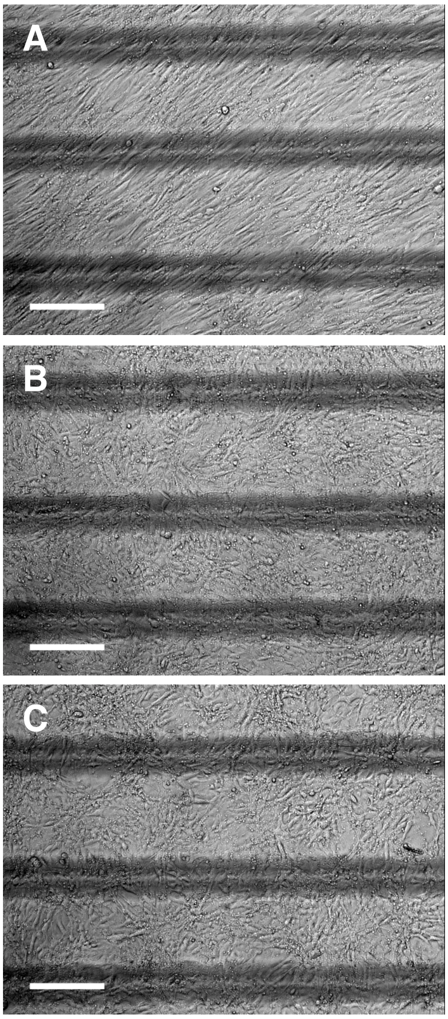

Online Figure IV. Cell orientation at confluence with stress fiber inhibition. A, Coherent orientation at confluence when cultured on FN/PEG substrates. The loss of coherent orientation on FN/PEG substrates with inhibitor (**B**) Y27632 or (**C**) blebbistatin. Scale bar, 200 μm.

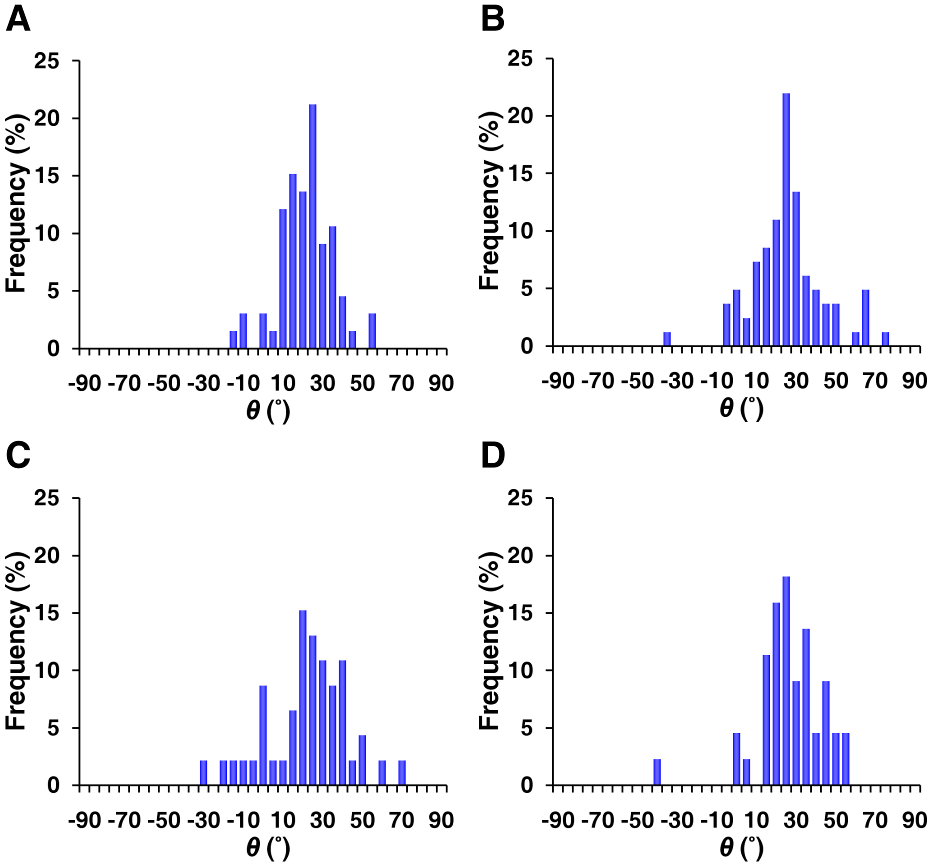

Online Figure V. Histogram of coherent orientation *θ* on FN/PEG stripes with various width. The stripe width is (**A**) 300 µm (20 ± 13.3°; n = 66 cells; mean ± s.d.), (**B**) 400 µm (24 ± 18°; n = 82 cells), (**C**) 500 µm (21 ± 20°; n = 46 cells), or (**D**) 600 µm (25° ± 17°; n = 44 cells). The images were taken on day 7.

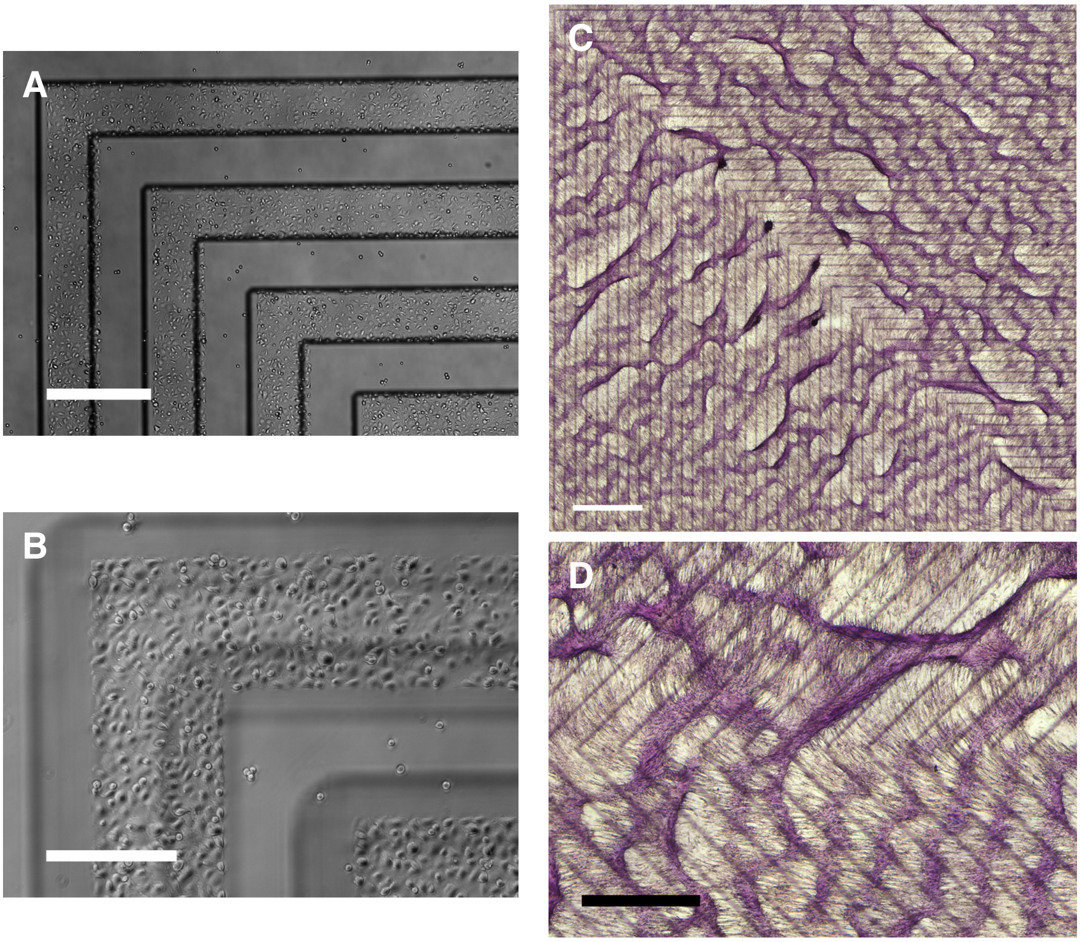

Online Figure VI. Transition of local alignment at the junction of two orthogonal sets of interfaces. Phase contrast microscopy of VMCs on FN/PEG substrates (interfaces identified by black titanium lines) at day 0 at (**A**) low magnification (scale bar, 600 µm) and (**B**) high magnification (scale bar, 300 µm). **C,** Light microscopy of hematoxylin-stained cells at day 12, showing alignment of aggregates in a stripe pattern at 110° relative to interfaces up to the edge of the transition zone, where nodules arose and cell alignment smoothly curved over a distance of about 300 µm. Scale bar, 2 mm. **D,** High magnification at the junction zone of two orthogonal sets of interfaces. Scale bar, 1.2 mm.

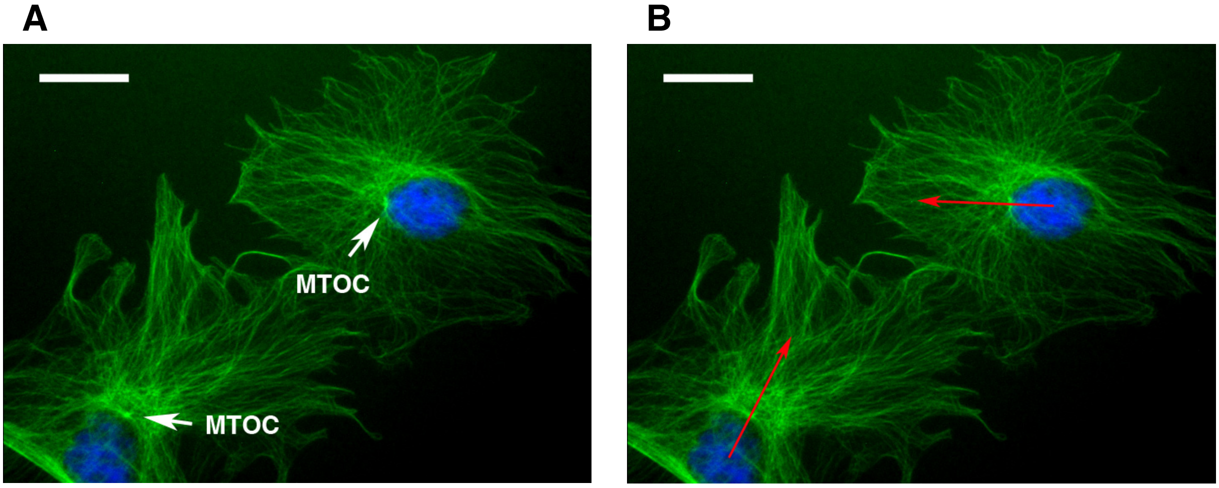

Online Figure VII. The polarity of VMCs. Immunofluorescence microscopy of α-tubulin in VMCs showing (**A**) MTOCs and (**B**) the direction of polarity (red arrow) based on MTOC orientation relative to the nuclear centroid. Scale bar, 20 μm.

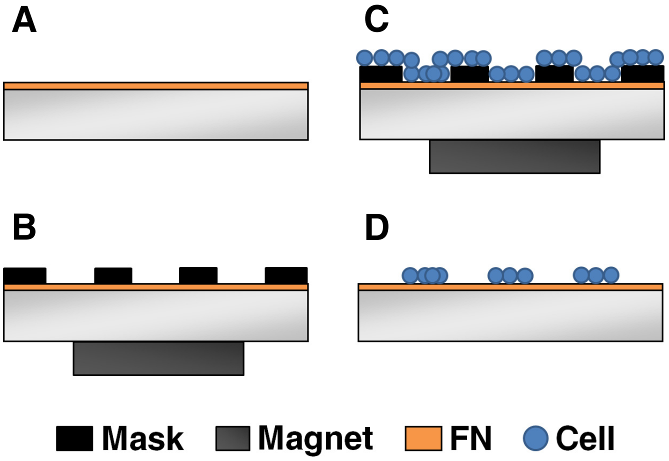

Online Figure VIII. Shadow-mask plating. A, Uniform coating of FN on the tissue culture dish. **B,** A magnet underneath the tissue culture dish immobilizes the shadow-mask above. **C,** Cell plating through the mask allows only cells within the windows to adhere to the FN. **D,** Cells remain in the specific domains of the windows after mask removal.

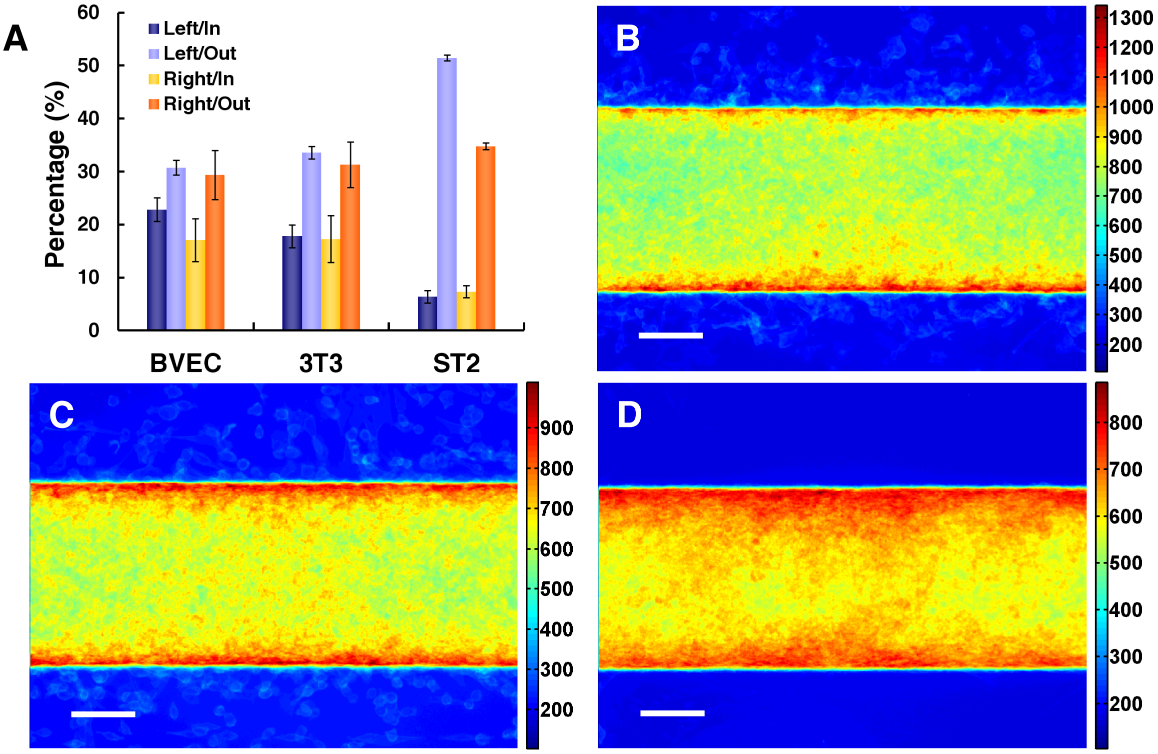

Online Figure IX. Stress fiber accumulation of BVECs, 3T3 cells and ST2 cells at FN/PEG interface. (**A**) Polarity of BVEC (n = 3; > 175 cells each), 3T3 (n = 5; > 245 cells each) and ST2 (n = 3; >265 cells each) near the FN/PEG interface. Stacked images of immunofluorescence microscopy of NMM-IIa in (**B**) BVECs (n = 45), (**C**) 3T3 fibroblasts (n = 50), and (**D**) ST2 cells (n = 35) on FN/PEG substrate. Scale bar, 100 µm.

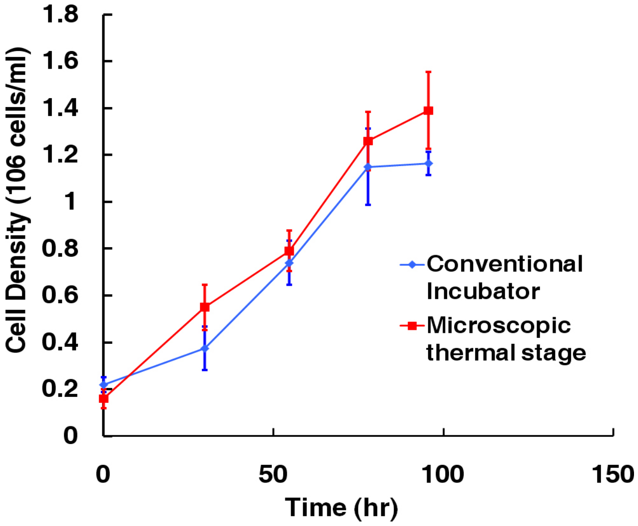

Online Figure X. Proliferation of 3T3 cells in a conventional incubator compared with that on a thermal stage (mean ± s.d.).

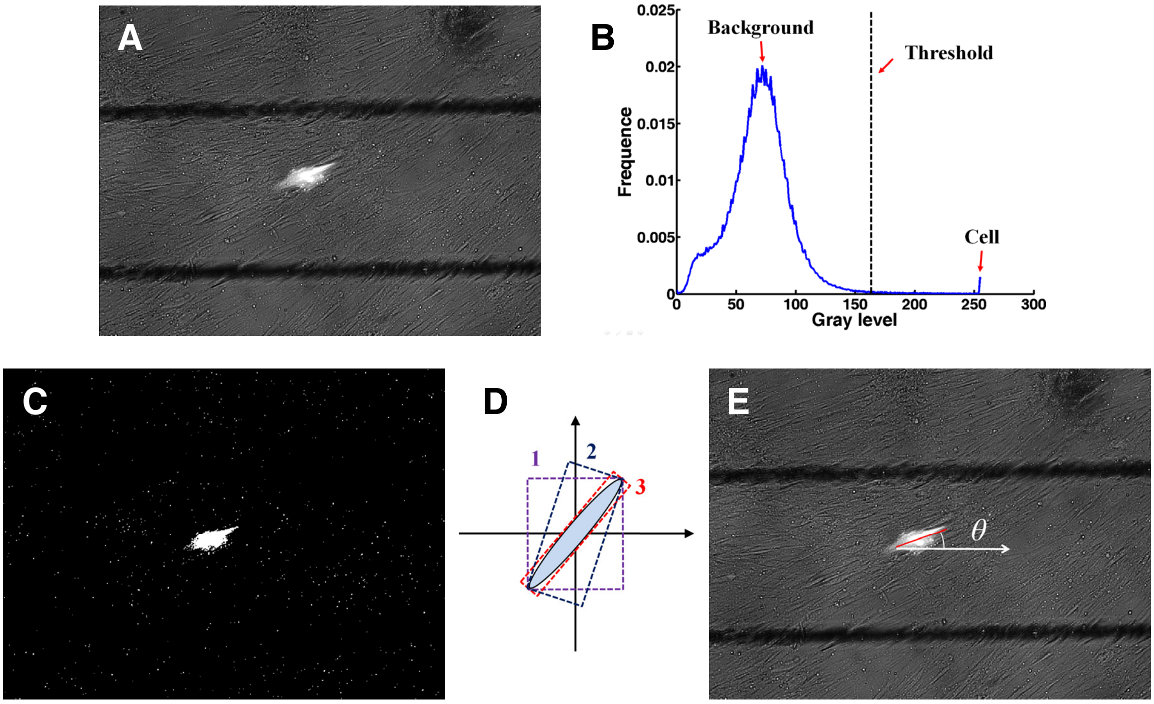

Online Figure XI. Image processing procedure for orientation analysis. **A,** The original gray scale image containing GFP-transfected cells. **B,** The histogram of the gray level in (**A**). **C,** Image segmentation with the threshold determined from the histogram of gray level. **D,** The orientation defined as the angle of the longitudinal axis of the minimal circumscribed rectangle relative to the horizon axis of the image. **E,** The original image superimposed on the calculated orientation angle θ.

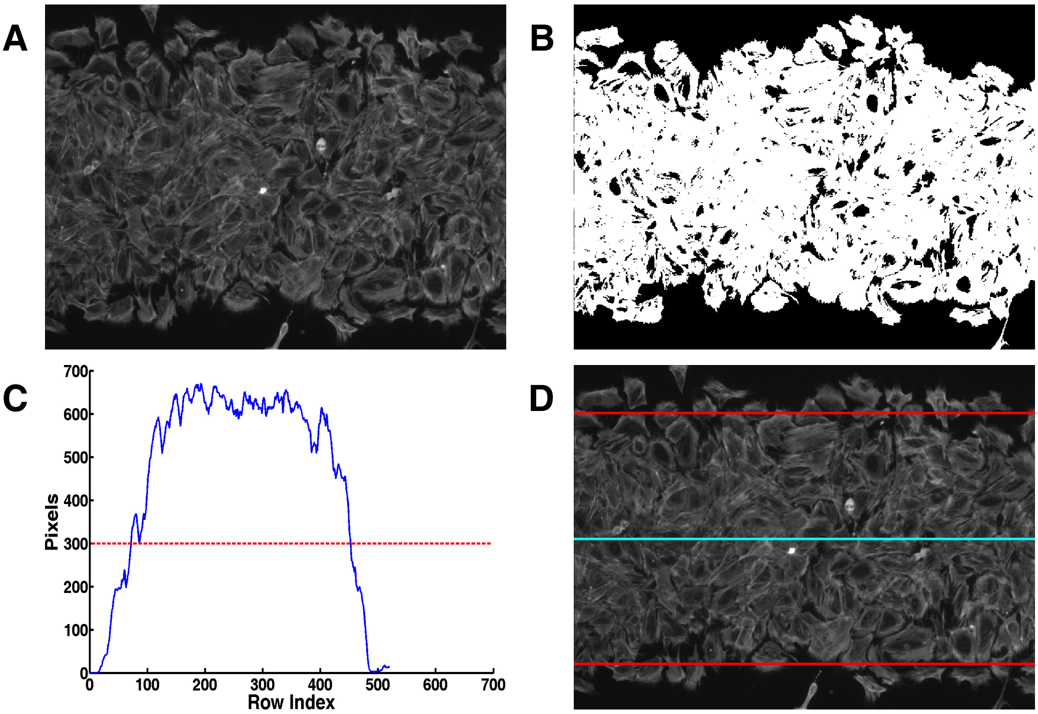

Online Figure XII. Image processing procedure for registration of NMM-IIa images from shadow-mask plating. **A,** The original gray scale image of immunofluorescence NMM-IIa. **B,** Image segmentation with exclusion of isolated cells. **C,** Number of bright pixels *vs.* row index of the image. The edges of cell sheet were identified by two intersections between the red dotted line (300 pixels) and the blue curve. **D,** Midline of cell sheet, defined as equidistant between the two edges, was used to register and stack the images.

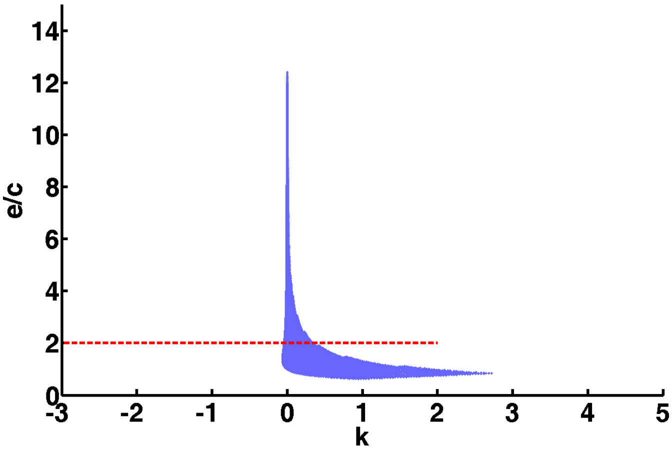

Online Figure XIII. The Turing space plotted as a function of *k* and *e*/*c*. The red dotted line represents $e/c = 2$, and the blue area represents the Turing space. The range of *k*, $0 < k < 0.34$, was determined by the span of the red dotted line which overlaps the blue area.

Supplemental References

1. Li N, Ho C-M. Photolithographic patterning of organosilane monolayer for generating large area two-dimensional B lymphocyte arrays. *Lab Chip.* 2008;8:2105-2112.

2. Bostrom K, Watson KE, Horn S, Wortham C, Herman IM, Demer LL. Bone Morphogenetic Protein Expression in Human Atherosclerotic Lesions. *J Clin Invest.* 1993;91:1800-1809.

3. Hsiai TK, Cho SK, Reddy S, Hama S, Navab M, Demer LL, Honda HM, Ho CM. Pulsatile flow regulates monocyte adhesion to oxidized lipid-induced endothelial cells. *Arterioscler Thromb Vasc Biol.* 2001;21:1770-1776.

4. Wong PK, Yu F, Shahangian A, Cheng G, Sun R, Ho C-M. Closed-loop control of cellular functions using combinatory drugs guided by a stochastic search algorithm. *Proc Natl Acad Sci U S A.* 2008;105:5105-5110.

5. Garfinkel A, Tintut Y, Petrasek D, Bostrom K, Demer LL. Pattern formation by vascular mesenchymal cells. *Proc Natl Acad Sci U S A.* 2004;101:9247-9250.

6. Painter KJ, Maini PK, Othmer HG. Stripe formation in juvenile Pomacanthus explained by a generalized Turing mechanism with chemotaxis. *Proc Natl Acad Sci U S A.* 1999;96:5549-5554.

7. Maini PK, McElwain DLS, Leavesley DI. Traveling wave model to interpret a wound-healing cell migration assay for human peritoneal mesothelial cells. *Tissue Eng.* 2004;10:475-482.

8. Witkin A, Kass M. Reaction-Diffusion Textures. Paper presented at: SIGGRAPH Computer Graphics; July, 1991; Las Vegas, NV, USA.

9. DiMilla PA, Quinn JA, Albelda SM, Lauffenburger DA. Measurement of Individual Cell Migration Parameters for Human Tissue Cells. *AIChE Journal.* 1992;38:1092-1104.

Legends for Video files

Online Video I. Time-lapse observation of cell migration over 22.5 hours. Cells coherently migrated following the orientation angle 22° relative to FN/PEG interface, gradually aggregating into parallel ridges perpendicular to the orientation.

Online Video II. Numerical simulation of $n(x, y)$ for isotropic cell migration ($b_1 = 1$, $b_2 = 1$).

Online Video III. This movie shows the numerical simulation of $n(x, y)$ for anisotropic cell migration ($b_1 = 1$, $b_2 = 10^{-6}$).